Chapter 5
Observing the Diffuse ISM: The Space Missions

In a new adventure of discovery no one can foretell what will be found, and it is probably safe to predict that the most important new discovery that will be made with flying telescopes will be quite unexpected and unforeseen.

—Lyman Spitzer, Jr. 1961,
Bulletin of the Atomic Scientists (May 1961), Vol. 17, No. 5, 194.

Abstract This chapter describes how space based observatories have influenced the study of the diffuse ISM by their opening of the full electromagnetic spectrum to imaging and spectroscopic study. From the radio to gamma-rays, satellites have contributed substantially heavily to the field. We review some of the more significant missions and describe some of their special capabilities for studying the diffuse ISM since many of these satellites have produced significant archival databases.

5.1 Introduction

During the last third of the 20^{th} century, astronomy underwent a third revolution in instrumentation, as great as the development of the telescope and spectroscope for astronomical observations had been. The opening of the electromagnetic spectrum finally allowed a complete view of astrophysical objects, not biased by the optical and radio windows. As UV, infrared, X-ray, and finally gamma-ray astronomy developed instruments and techniques to study the sky, the nature of astrophysical research changed—just compare an issue of *The Astrophysical Journal* from 1966 to one from 2016. Of course, part of the problem in developing the instrumentation necessary to explore the portions of the electromagnetic spectrum outside of the optical and radio regimes is the opacity of the Earth's atmosphere. This was finally surmounted by space-based instrumentation following the development of rocketry in the 1950s and 1960s.

L. Magnani, S.N. Shore, *A Dirty Window*, Astrophysics and Space Science Library 442, DOI 10.1007/978-3-662-54350-4_5

This third instrumental revolution in astronomy had, and has, a profound impact on our view of the diffuse ISM. We will survey some of the most salient results in this area in the last four decades, with the understanding that the next four decades will be even more exciting.

5.2 The Radio Regime

Radio astronomy is traditionally done via ground based telescopes and arrays but there have been a few space missions involving radio antennas and instrumentation. At the lowest frequencies, RADIOASTRON (aka Spektr-R) is a joint ground-space VLBI project led by the Astro Space Center of the Lebedev Physical Institute of the Russian Academy of Sciences. It features a 10 m antenna on board an Earth-orbiting satellite which can be coupled with ground-based radio telescopes to produce interferometric baselines of up to 390,000 km. It operates at wavelengths of 1.35–6, 18, and 92 cm. and is used to study the structure of active galactic nuclei, pulsars, and masers. With its 10 m antenna, it is the largest orbiting radio telescope.

Single-dish radio telescopes are, in general, not suitable for space-based platforms because of size considerations and the associated angular resolution issues, but, recently, satellites such as COBE, WMAP and *Planck* featured telescopes that straddled the mm-submm region of the electromagnetic spectrum. In particular, the *Planck* mission[1] had sufficient resolution that it could be considered a mm-wave orbiting telescope and, as such, we discuss some of its initial results relevant to the diffuse ISM.

5.2.1 The Planck Observatory

The *Planck* Observatory, an ESA mission with significant NASA involvement, was launched in an Earth-Sun L2 orbit in May 2009 to survey the sky for both continuum and spectral lines in the range 30–857 GHz with angular resolution from $33'$ to $5'$. *Planck's* primary goal was to study the CMB and, as such, it was the third generation mission to do so after the COBE and WMAP satellites. It functioned from May 2009 to January 2012 with the Low Frequency Instrument (LFI) observing at wavelengths greater than 4 mm. Its 100 GHz channel can be used to trace CO(1-0) emission (115.27 GHz), but it is "contaminated" by ^{13}CO (1-0) emission (110.20 GHz) and CMB emission. Similarly, the CO(2-1) line contributes to the 217 GHz channel, and

[1] http://www.esa.int/Planck.

the CO(3-2) line to the 353 GHz channel. This last channel is sometimes called the "dust" channel because it picks up a lot of thermal emission from cold dust. The CO emission in the 100 GHz channel had to be calibrated so that the ^{13}CO and CMB contributions could be removed (Planck Collaboration, Planck 2013 Results, 2014, Paper XIII; Planck Collaboration, Planck 2013 Results XIII 2014). This was done by comparing its emission data to CO datasets from the Harvard-Smithsonian CfA 1.2 m, the Nanten 4 m, and the FCRAO 14 m radiotelescopes, and the CMB data from COBE/FIRAS.

The Planck Collaboration discussed the relationship between molecular gas and dust emission in several early papers (Planck Collaboration, Planck Early Results 2011, Papers XXI, XXII, XXIII, XXIV, XXV) (Planck Collaboration, Planck Early Results XXI 2011; Planck Collaboration, Planck Early Results XXII 2011; Planck Collaboration, Planck Early Results XXIII 2011; Planck Collaboration, Planck Early Results XXIV 2011; Planck Collaboration, Planck Early Results XXV 2011) and mapped the entire sky in the lower CO rotational transitions (Planck Collaboration, Planck 2013 Results, 2014, Paper XIII) (Planck Collaboration, Planck 2013 Results XIII 2014). Figure 5.1 shows an early release of the *Planck* 100 GHz data for the whole sky showing primarily CO(1-0) emission, along with that from ^{13}CO(1-0) and the CMB. Although the resolution is only 10′, this is the only complete all-sky map in any molecular tracer and, as such, provides the

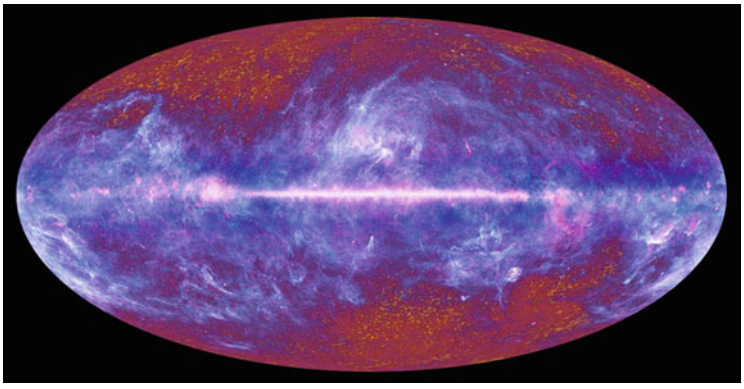

Fig. 5.1 *Planck* whole-sky survey at 100 GHz after one year of data collection. The 100 GHz channel features primarily the CO(1-0) emission from molecular clouds (blue/white regions), but the ^{13}CO(1-0) line is also present. In addition, temperature variations from the CMB are visible at the highest latitudes. Compare to Fig. 7.3 which removes the ^{13}CO and CMB contributions. The image is from the ESA/Planck collaboration

most complete view of the molecular Milky Way to date. The Harvard-Smithsonian Center for Astrophysics molecular map of the sky has 8′ resolution and the telescope is continuing to map the sky accessible from Cambridge, Massachusetts (see www.cfa.harvard.edu/mmw/).

While the sensitivity of the *Planck* maps is adequate to study the molecular emission from GMCs and the larger clouds, the more diffuse and translucent molecular gas is not as well defined. Figures 5.2, 5.3, 5.4, 5.5, 5.6, 5.7 show a translucent and a diffuse molecular cloud (see Chap. 8 for definitions) as mapped in CO by conventional ground-based mm-wave telescopes, by the *Planck* CO channel (100 GHz) and the *Planck* dust channel (353 GHz). Without ^{13}CO and CMB removal, the 100 GHz channel barely shows the outline of the clouds, but at 353 GHz the dust emission detected by *Planck* (e.g., Fig. 5.3) tracks both the IRAS 100 μm (Fig. 5.2 right) and the CO(1-0) emission (Fig. 5.2 left). With its comprehensive frequency and sky coverage, the CO maps from *Planck* are an invaluable contribution to our knowledge of the large-scale molecular gas distribution in the Galaxy.

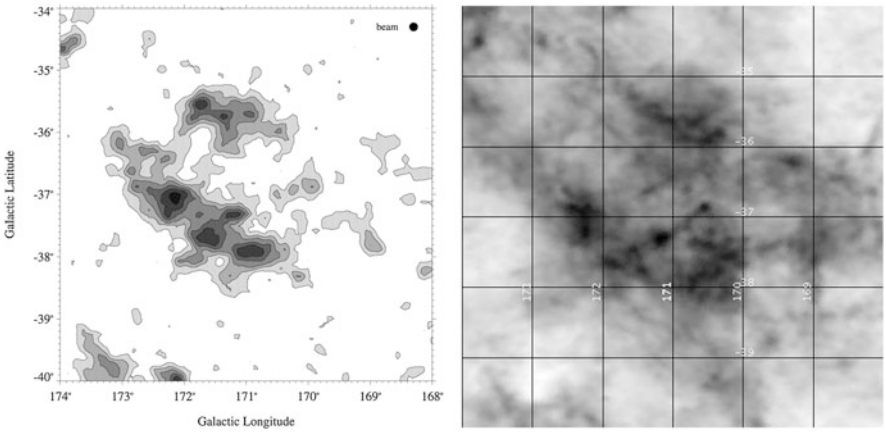

Fig. 5.2 CO and dust comparison for region centered on the high-latitude cloud MBM 16. On the left, CO(1-0) contour map made with 1.2 m mm-wave telescope of the Harvard-Smithsonian Center for Astrophysics. The velocity range of the map is $-10\,\mathrm{km\ s^{-1}} \leq v_{LSR} \leq 15\,\mathrm{km\ s^{-1}}$ and contour levels are 15%, 30%, 45%, 60%, 75%, and 90% of the maximum integrated CO antenna temperature of 6.5 K km s^{-1}. The map is fully-sampled and the resolution is 8.4′. For more details, see Magnani et al. (2003). On the right, a similarly sized map centered on MBM16, showing emission from the IRIS 100 μm data that primarily traces thermal dust. The gray scale is a log scale and ranges from 5.60 to 26.48 MJy/ster. The image was made with the Skyview Virtual Observatory

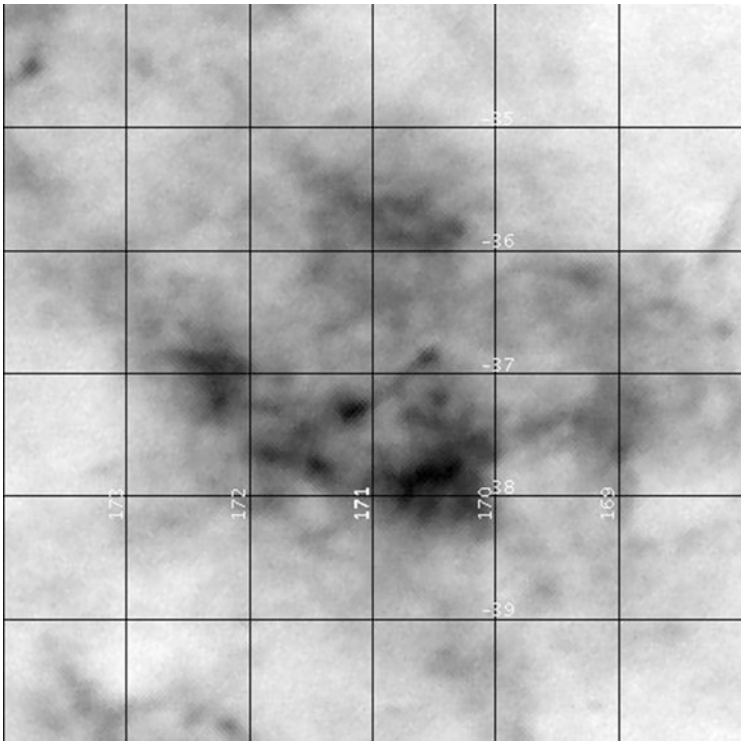

Fig. 5.3 Same region as in Fig. 5.2, centered on MBM16, showing emission from the *Planck* 353 GHz channel which primarily traces dust. The gray scale is linear and ranges from 1.92×10^{-3} K to 12.25×10^{-3} K. The image was made with the Skyview Virtual Observatory

In addition to the CO maps, the three highest frequency *Planck* channels (857, 545, and 353 GHz) can be used to cover the peak thermal emission from dust regions colder than 14 K, and Planck Collaboration, Planck Early Results 2011, Paper XXIII Planck Collaboration, Planck Early Results XXIII 2011 produced the first all-sky survey of Galactic cold clumps. The cold sources they detected included a range of objects from low-mass dense cores to GMCs, so their use of the word "clump" is far more encompassing than what is normally considered a clump in the ISM. There is little question, however, that these sources are associated with molecular gas. A detailed analysis of the clump distribution with the CO(1-0) intensity map just described showed that 95% of the clumps are associated with CO structures (see also Planck Collaboration, Planck 2015 Results, Paper XXVIII Planck Collaboration, Planck 2015 Results XXVIII).

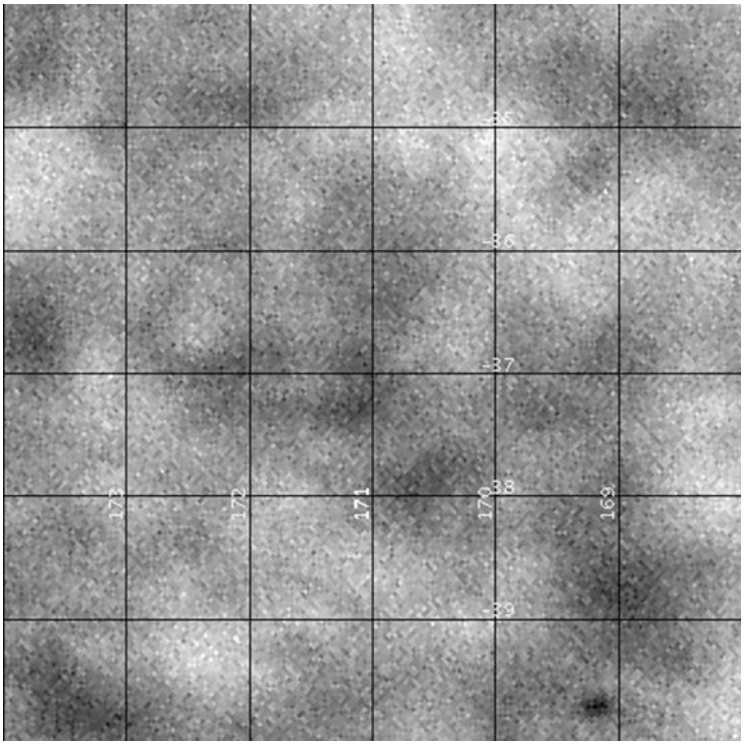

Fig. 5.4 Same region as in Figs. 5.2 and 5.3, centered on MBM16, showing emission from the *Planck* 100 GHz channel which traces emission from the CO(1-0) transition, the CMB, and ^{13}CO(1-0). Notice the contrast between this image and the CO(1-0) map in Figure 5.2, highlighting the effect of the broad band contamination relative to high-spectral resolution studies. The gray scale is linear and ranges from -3.47×10^{-4} K to 7.71×10^{-4} K. The image was made with the Skyview Virtual Observatory

With the ability to trace both CO and dust components, the *Planck* team addressed the issue of "dark" molecular gas (see Sect. 8.4) and proposed that it can correspond up to as much as 28% of the atomic mass and contribute even more molecular mass (118%) in the solar neighborhood than currently determined from conventional CO(1-0) observations (Planck Collaboration, Planck Early Results 2011, Paper XIX)(Planck Collaboration, Planck Early Results XIX 2011). These results were preliminary and are more than likely overestimates—especially for the molecular case. We revisit the issue in Chap. 8.

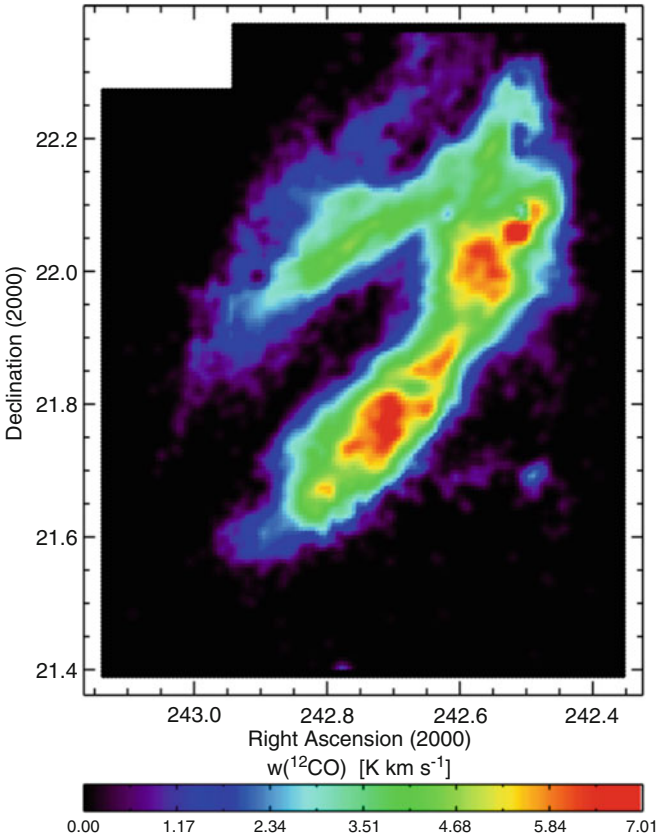

Fig. 5.5 CO(1-0) map in color of the core region of MBM 40 (Chastain 2005). The units are velocity-integrated antenna temperature with the color scale at the *bottom*. The CO data were taken with the FCRAO 15-m telescope and have a resolution of 45″ and are fully-sampled. The 1-σ rms of the antenna temperature is only 0.7 K so there is much more low-level CO emission in this region. See discussion by Cotten and Magnani (2013)

5.2.2 WMAP

The Wilkerson Microwave Anisotropy Probe was launched in June 2001 to make fundamental cosmological measurements of the CMB. It made all-sky maps at 22, 30, 40, 60, and 90 GHz at resolutions of 0.93, 0.68, 0.53, 0.35 and <0.23 degrees, respectively (see Fig. 1.5 for the all-sky map at 40 GHz). In the process

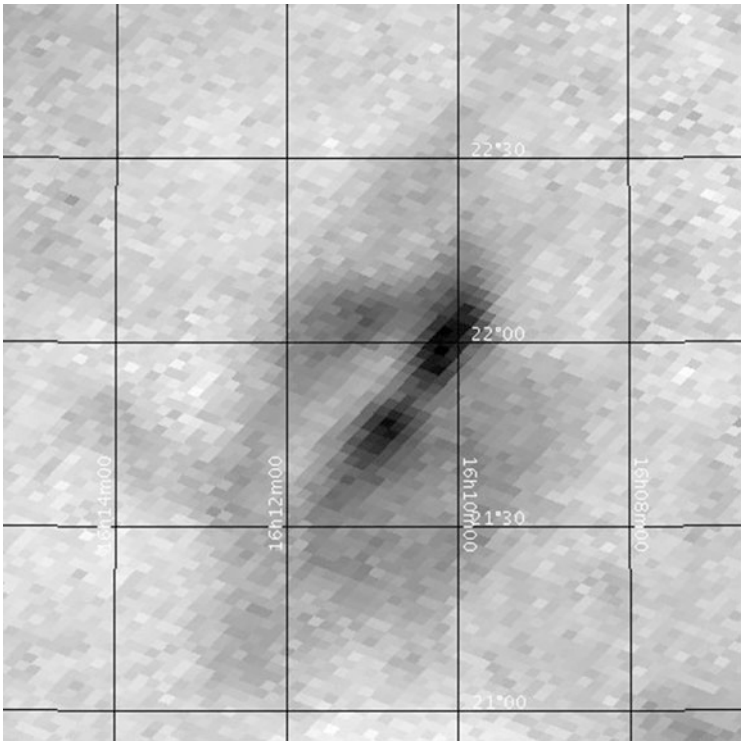

Fig. 5.6 Region centered as in Fig. 5.5 but twice the size, showing emission from the *Planck* 353 GHz channel which primarily traces dust. The gray scale is linear and ranges from 4.94×10^{-4} K to 4.924×10^{-3} K. The image was made with the Skyview Virtual Observatory. Notice how the broadband contamination of ^{13}CO and CMB effectively obliterate the cloud

of obtaining the data so valuable for the CMB, the satellite also picked up Galactic synchrotron and free-free radiation, and some thermal radiation from interstellar dust. A fourth Galactic component, Anomalous Microwave Emission (AME), thought to arise from spinning dust is still somewhat controversial as regards its production mechanism (Sect. 3.5.3). Regardless of its provenance, AME does exist over the frequencies covered by WMAP. This was clear when the Galactic emission from the three established components was removed and there was still a correlation with the dust component associated with the infrared cirrus (Kogut et al. 1996; Leitch et al. 1997). This anomalous emission is discussed further in Sect. 6.6.3 .

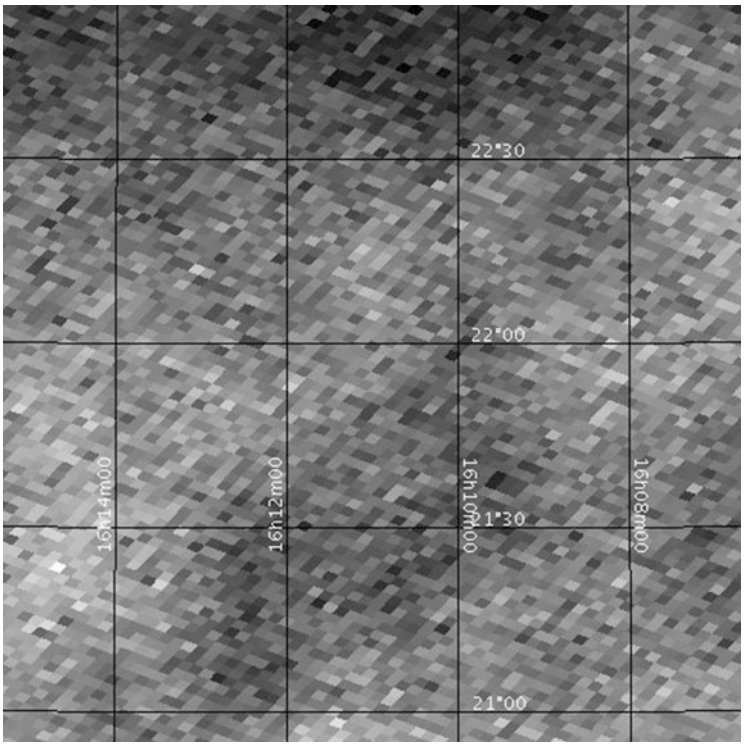

Fig. 5.7 Region centered as in Fig. 5.5 but twice the size, showing emission from the *Planck* 100 GHz channel which traces CO(1-0), the CMB, and ^{13}CO(1-0). The gray scale is linear and ranges from -1.76×10^{-4} K to 4.66×10^{-4} K. Because the CO(1-0) emission in the densest region of MBM 40 is greater than in MBM 16, and the 100 and 353 GHz emission lower, it is likely the gas-to-dust ratio in MBM 40 is higher than in MBM 16 (compare Figs. 5.2–5.4 with Figs. 5.5–5.7). Notice how the broadband contamination of ^{13}CO and CMB effectively obliterate the cloud. The image was made with the Skyview Virtual Observatory

5.3 Probing the Infrared Sky

With the development of infrared detectors and their deployment on satellites providing large-scale mapping of the sky in near and far infrared, Galactic dust can no longer hide anywhere and its properties can be determined with unparalleled precision. It is safe to say that we are just at the beginning of the returns from the opening of the infrared window. The dust and gas in the ISM are well-mixed (Spitzer 1978) with a typical gas to dust ratio, by mass, of about 100. Despite representing

only about 1% of the mass of the ISM, the dust is easy to detect (once infrared-detection technology was developed) and gives remarkable views of the structure and distribution of the diffuse ISM. In the next section we briefly review some of the more important infrared space missions for tracing dust in the diffuse ISM.

5.3.1 IRAS

The Infrared Astronomy Satellite (IRAS) was launched on January 25, 1983. This date can be taken as the dawn of a new way to study the ISM. The IRAS mission was initiated in the mid-1970s as a joint project by the United States, the Netherlands, and the United Kingdom. Its principal goal was to produce an unbiased, uniform survey of the entire sky at four infrared wavelengths centered at 12, 25, 60, and 100 μm. The satellite ceased operations in November 1983 when the liquid helium that cooled the telescope had evaporated away. By the end of the mission, it was clear that the IRAS survey was a great success with more than 96% sky coverage [for more details, see Neugebauer et al. (1984), and the IRAS Explanatory Supplement (1988)]. The principal data products of the project were the compilation of a catalog of infrared point sources, a catalog of extended sources less than 8′ in extent, and an atlas of calibrated images of nearly all of the infrared sky. The resolution of these images was 2′ at 100 μm, but, later, reprocessed versions of the original images which resolved several troublesome calibration issues had spatial resolution in the 4′–6′ range.

The impact of the results on the astronomical community was tremendous. Rumors of exciting new findings circulated throughout the summer of 1983, but the proprietary nature of the data prevented external researchers from examining any of the images. The initial, spectacular results of the mission were presented in the March 2004 issue of *The Astrophysical Journal Letters* (Vol. 278). Among the discoveries were distant, powerful infrared galaxies fueled by prodigious rates of star formation, a shell of dust around α Lyrae, surprisingly strong infrared emission from Arp 220, a new comet, and an extended emission component visible at high Galactic latitude primarily at 60 and 100 μm. The extended emission was dubbed "infrared cirrus" because of the ragged nature of the structures which—at some level—covered most of the high-latitude sky.

Although the IRAS discovery of the infrared cirrus (Low et al. 1984) was momentous, the lack of velocity information left open *where* it was located. While most of the authors of the paper announcing the discovery would have favored a Galactic origin, caution forced the inclusion of the following statement:

This dust emission could, perhaps, be associated with HI at anomalous velocities, with small amounts of molecular rather than atomic hydrogen, or with cold material in the outer solar system. Fortunately, the IRAS mission plan of rescanning the sky after an interval of 6 months is well suited to distinguish between dust clouds in orbit around the Sun at various distances and distant interstellar clouds. This aspect of

the infrared cirrus remains one of the most enigmatic characteristics of the sky as seen by IRAS and will continue as such until the sky has been examined a second time.

Within two years, the identification of the high-latitude cirrus with a local, Galactic component was firmly established by Weiland et al. (1986). Along with the cirrus, another IRAS discovery of relevance to our discussion was the somewhat surprising amount of infrared emission from the cirrus at 12 and 25 μm. This type of emission was associated with temperature "spikes" as very small grains or PAHs absorb individual, high-energy photons (Sellgren 1984; Boulanger et al. 1985; Puget et al. 1985; Draine and Anderson 1985, Omont 1986, Desért et al. 1986).

Although the infrared data from the IRAS mission is now over three decades old, it is still used productively and offers the simplest and quickest way to look at the dust distribution in the Galaxy (i.e., through the Skyview Virtual Observatory: http://skyview.gsfc.nasa.gov/current/cgi/titlepage.pl).

An improvement to the original data was made by reprocessing the data to better remove the pesky zodiacal light contribution, calibrating and fixing zero levels so as to be compatible with the DIRBE instrument on the COBE satellite[2] (see below), and improving the destriping algorithms. The resulting database is called IRIS and with its 4′ resolution matching the *Planck* high frequency bands, it provides an outstanding view of the dust emission from the Galaxy (Miville-Deschênes and Lagache 2005). Figures 5.2 (right) and 5.8 show IRIS 100 μm data for the translucent cloud MBM 16 and the diffuse molecular cloud MBM 40, respectively. The figures should be compared to Fig. 5.3 and Fig. 5.6 which are the *Planck* 353 GHz (which is equivalent to 849 μm) data for the regions in question.

5.3.2 COBE and ISO

The COsmic Background Explorer (COBE) was launched by NASA on November 18, 1989 primarily to study the CMB in the infrared. It provided the best measurements of the CMB spectrum of that time and revealed the fluctuations in temperature at the 10^{-5} level (which garnered George Smoot and John Mather the Nobel Prize in physics in 2006). Galactic dust emission was also detected by the instruments on board the satellite with better calibration than IRAS, although with lower angular resolution. In particular, the Diffuse InfraRed Background Experiment (DIRBE) and the Far InfraRed Absolute Spectrophotometer (FIRAS) instruments carried forward the legacy of IRAS and led to several important developments.

DIRBE was a photometer with ten bands covering the range from 1.25 to 240 μm at a somewhat poor resolution of 40′ (Silverberg et al. 1993). The FIRAS instrument was a polarising Michelson interferometer with an angular resolution of 7° and a

[2]The IRAS mission also served as the pathfinder for COBE, in the sense that analysis of the IRAS data led to models of the Galactic dust component.

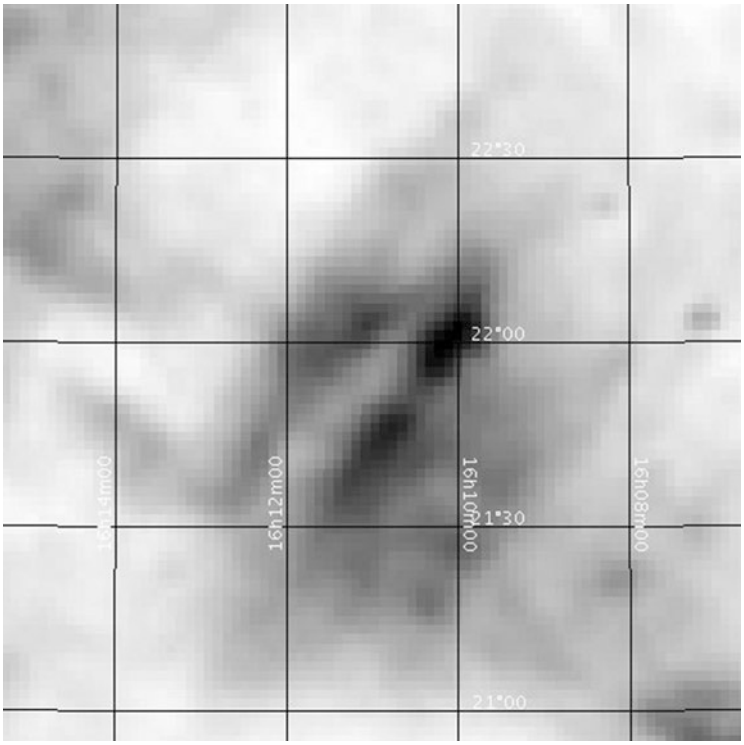

Fig. 5.8 Region centered as in Fig. 5.5 but twice the size ($2^\circ \times 2^\circ$), showing emission from the IRIS 100 μm data which primarily traces thermal dust. The image is centered at (RA, Dec) = (16^h 11^m 00^s, 21° 55' 00") in 2000.0 coordinates. The gray scale is a log scale and ranges from 3.21 to 11.76 MJy/ster. The image was made with the Skyview Virtual Observatory

fixed spectral resolution in two separate bands of 0.57 cm^{-1} (Fixsen et al. 1994). The high-frequency band (from 20 to 96 cm^{-1}) was also used to study the Galactic thermal emission. Although the resolution of this instrument was somewhat poor (0.7 degrees), its careful calibration was very useful in reprocessing IRAS data. For example, the Schlegel et al. (1998) dust maps were based on the DIRBE calibrations.

The Infrared Space Observatory (ISO) was an infrared satellite observatory built by the European Space Agency (ESA) and launched in November of 1995. Its cryogenic reserves lasted until April of 1998 and the instruments on board allowed for observations in the 2.5–240 μm wavelength range (Kessler et al. 1996) and consisted of two spectrometers (SWS and LWS), a camera (ISOCAM), and an imaging photo-polarimeter (ISOPHOT). The spatial resolutions ranged from 1.5″ to 90″ and represented a distinct improvement over the previous missions, although an all-sky survey was precluded. Instead, some 30,000 individual imaging, photometric, spectroscopic, and polarimetric observations of various objects were made. The ISO archive can be accessed at http://iso.esac.esa.int/ida/.

5.3.3 *Spitzer, Herschel, and WISE*

The *Spitzer* Space Telescope (Werner et al. 2004) is the fourth and final of the NASA Great Observatories. It was launched in August 2003 and is still operating. Although primarily designed to study protoplanetary and planetary debris disks, brown dwarfs, and ultra-luminous infrared galaxies, the wavelength range of the instruments is such that interstellar dust can be readily studied (3.6, 4.5, 5.8, 8, 24, 70, 160 μm). Although the liquid helium ran out in May 2009, the mission continues with the two shortest wavelength modules of the IRAC camera (3.6 μm and 4.5 μm still operating and taking data as part of the Spitzer Warm Mission) with a field of view of $5' \times 5'$ and an angular resolution of $1.9''$. While it was cryogenically cooled, IRAC also operated at 5.8 μm and 8 μm.

The telescope consists of an 85 cm mirror and instrumentation to observe the cosmos from 3.6 to 180 μm. Besides the IRAC, Spitzer was also equipped with a Multiband Imaging Photometer (MIPS) which produced images at 24, 70, and 160 μm. The size of the images varied from $5' \times 5'$ at 24 μm to $0.5' \times 5'$ μm at 70 μm. In addition to the imaging cameras the Infrared Spectrograph (IRS) was capable of both high- and low-resolution spectroscopy at mid-IR wavelengths (5–40 μm). This range makes the data particularly useful for studying PAHs in the ISM.

Of particular interest for the diffuse interstellar medium is the *Spitzer*/GLIMPSE survey of the Milky Way (Churchwell et al. 2004). Three large surveys were undertaken. The first fully mapped the Galactic plane at 3.6, 4.5, 5.8, and 8.0 μm for $\ell = 10° - 65°$ and $|b| \leq 1°$ with a spatial resolution of less than $2''$. The second survey fully imaged the inner 20° of the Galactic plane, and the third surveyed the central bar by extending the latitude coverage to $|b| \leq 3°$.

The *Herschel* Space Observatory was an ESA project and consisted of a single 3.5 m telescope with instrumentation that covered the far-infrared and submillimeter bands from 55 to 672 μm. The *Herschel* mission lasted from May 2009 to April 2013. At the time, it was the largest mirror ever deployed in space. The telescope was placed in an Earth-Sun L2 orbit with imaging instruments that included the Photodetecting Array Camera and Spectrometer (PACS) covering wavelengths from 55 to 210 μm and the Spectral and Photometric Imaging Receiver (SPIRE) covering the wavelength range from 194 to 672 μm. Both instruments also served as low-resolution spectrometers, but the high-resolution spectral work was done by the Heterodyne Instrument for the Far Infrared (HIFI). *Herschel* obtained observations of sub-mm transitions of molecules, and the PRIMAS project took advantage of this to survey transitions of the ions CH^+, SH^+, OH^+, OH_2^+, and OH_3^+; and of the neutrals OH, H_2, NH, NH_2, NH_3, and HF. An entire issue of the journal *Astronomy and Astrophysics* was devoted to its initial results.[3] With its great resolution and sensitivity, *Herschel* provided a fantastic instrument for studying individual objects in the infrared.

[3] *Astronomy & Astrophysics*, Volume 518, July–August 2010.

The *Wide-field Infrared Survey Explorer* (WISE) was launched in December 2009, placed in hibernation (by turning off its transmitter in February 2011), and re-activated in August 2013. In the first phase of its mission, it functioned as an infrared telescope (40 cm diameter) conducting an all-sky survey at 3.4, 4.6, 12 and 22 μm. Once its coolant was depleted, it spent it remaining time searching for near-Earth objects. In its second phase mission, it is recommissioned (NEOWISE) to search for near-Earth asteroids. From its original mission, each image covers fields $47'$ in size with angular resolution of $6''$. Although the resolution is worse than that of *Spitzer* at 3.6 and 4.5 μm, its all-sky survey provides an excellent way to study the dust distribution in the diffuse ISM (see Fig. 5.9).

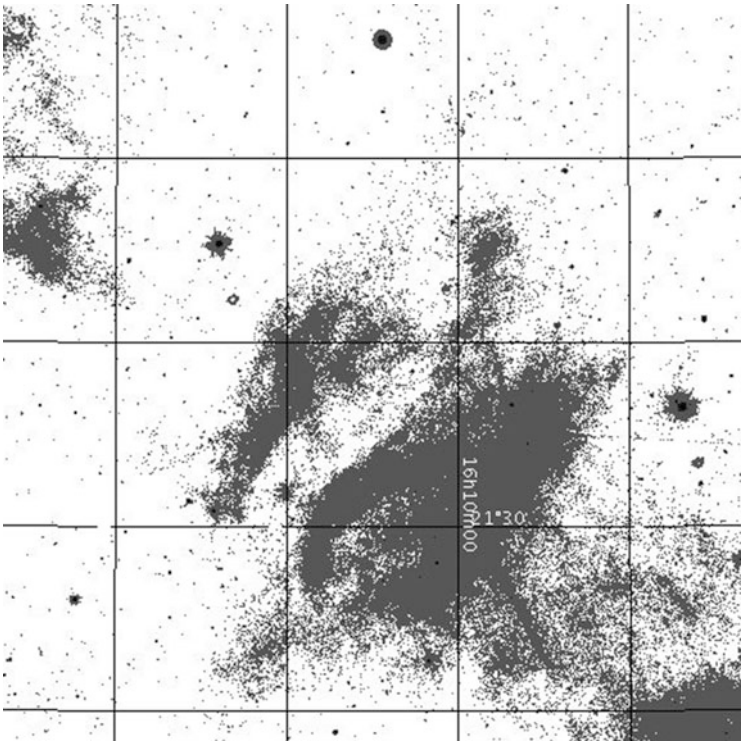

Fig. 5.9 Region centered as in Fig. 5.5 but twice the size ($2° \times 2°$), showing emission from the WISE 12 μm band. The image is centered at (RA, Dec) = ($16^h\ 11^m\ 00^s$, $21°\ 55'\ 00''$) in 2000.0 coordinates. The gray scale is a histogram equalization scale to highlight low-level extended emission and ranges from 420 to 3690 Digital Numbers (DN) units. The image was made with the Skyview Virtual Observatory

5.4 Spectral Tracers of Diffuse Molecular Gas in the Far-Infrared

In Chap. 3 we looked at various spectral tracers of diffuse molecular gas in the radio portion of the spectrum. The lines we highlighted were molecular, rotational or hyperfine transitions. In the infrared, the atomic fine structure lines of neutral carbon, CI, and singly-ionized carbon, CII, are the most important because of their visibility in the infrared from space-born platforms in the 1990s.

Along with CO, C^+, is the principal coolant in translucent and diffuse molecular clouds. Thus, lines from this species should be readily detectable in the diffuse, low-density molecular component of the ISM. Moreover, the $^2P_{3/2}$-$^2P_{1/2}$ transition of singly-ionized carbon at 157.7 μm is the dominant coolant in the CNM (see Sect. 1.5.4). In PDRs, C^+ is most abundant at the interface with the atomic ISM and thus the outermost envelope of any cold atomic or molecular cloud will show emission from this coolant. The 158 μm emission as observed by FIRAS aboard the COBE satellite shows strong correlation with neutral atomic hydrogen (Bennett et al. 1994). However, in dense molecular gas the [CII] emission is expected to drop-off as the carbon transforms to C^0 and CO and the UV heating of the grains decreases since the radiation fails to penetrate the more opaque clouds. Even in diffuse and translucent clouds, the [CII] intensity decreases relative to the surrounding diffuse atomic gas. Models indicate that the decrease in 158 μm is produced by attenuation and softening of the ISRF and not from a changes in the dust (Ingalls et al. 2002). In addition, observations of this transition can be used to obtain the median density and pressure in molecular regions.

Two fine structure transitions of CI are the $^3P_1$-$^3P_0$ line at 492 GHz and the $^3P_2$-$^3P_1$ line at 809 GHz. The former transition has been detected in the high-latitude molecular cloud, MBM 12, from ground-based observations by Ingalls et al. (1994—see also, Ingalls 1999). The ratio of C/CO in translucent clouds is expected to be around unity, significantly higher than toward dense Galactic PDRs. Although the column densities of neutral carbon are high, it is relatively difficult to carry out these observations from the ground and CO remains by far the favored tracer of these regions.

The *Stratospheric Observatory for Infrared Astronomy* (SOFIA) currently (2017) offers the best way to obtain infrared spectra and images from the near to the far infrared.[4] Although not a space mission, the observatory consists of a 2.5 meter Bent Cassegrain that is housed in a Boeing 747SP. The plane can fly at altitude of up to 13.7 km where it is above almost all the water vapor in the Earth's atmosphere. The project is a joint venture between NASA and the German Aerospace Center (DLR) and is a successor to the *Kuiper Airborne Observatory* (KAO).

[4] see https://www.nasa.gov/mission_pages/SOFIA/.

5.5 Probing the Ultraviolet Sky

Observations of absorption lines from electronic transitions in the UV portion of the spectrum are analyzed in the same way as optical absorption observations described in the Chap. 3; the key difference is that the observations must be conducted from earth orbit because of the opacity of the Earth's atmosphere to UV radiation. In the ISM, the widespread presence of atomic hydrogen effectively terminates UV observations below the Lyman limit (912 $\AA$).

The first observation of H_2 were from sounding rocket flights (Carruthers 1970), and the UV transitions of CO were detected immediately after (Smith and Stecher 1971). These discoveries paved the way for the *Copernicus* satellite (operated from 1972 to 1980) which produced most of the early information on the abundance and excitation of H_2 in the diffuse ISM (Spitzer et al. 1973). A key project for *Copernicus* was the survey of atomic and molecular hydrogen towards 109 stars leading to the two classic papers by Savage et al. (1977) and Bohlin et al. (1978) (see §2.3.1).

For the diffuse ISM, the absorption lines are produced as molecules in the ground electronic state absorb UV photons and transition to excited electronic states. Unfortunately, the dust in the ISM is an excellent absorber and scatterer of these photons—with increasing efficiency toward the shorter UV wavelengths, so that observations are possible only in regions with less than a magnitude of visual extinction (the corresponding extinction in the UV is anywhere from a few times to 15 times higher depending on the wavelength). Nevertheless, a lot of interesting work was done in the near UV from the ground. Notable UV observations of the diffuse ISM include observations of the OH line at λ3078Å by Crutcher and Watson (1976), NH, CH, and OH for the line of sight to ζ Per, all below 3400 Å (Chaffee and Lutz 1977), five OH transitions out of the $X^2\Pi_{3/2}$ ground state between 3070 Å and 3080 Å (Felenbok and Roueff 1996), FUSE observations of the line of sight to HD 34078 (Boissé et al. 2005), and OH observations towards 10 sightlines by Weselak et al. (2009).

The H_2 ground state consists of both electrons in the lowest 1sσ orbital and it is denoted by $^1\Sigma^+$. In the ultraviolet, the Lyman absorption lines from the ground state to the higher $^1\Sigma$ states were observed by space telescopes such as *Copernicus* in the 912 Å-1215 Å range against background early-type stars. But if one wishes to observe lines in emission, the lowest rotational levels in the $v = 0$ state are the only ones that are populated under the physical conditions of the diffuse ISM. However, because of selection rules, the transitions between odd and even J levels are forbidden. Thus, H_2 has para and ortho levels corresponding to even and odd J levels with transitions allowed only within each set of levels. The selection rules allow only those transitions with ΔJ = 2 so that the lowest allowed transition is the para J = 2-0 transition at 28 μm. Unfortunately, the J = 2 level is 500 K above the ground level and thus is not very populated in cold molecular clouds, although some observations of this transition have been made in shocked gas regions.

Notable UV telescopes after *Copernicus* were the *International Ultraviolet Explorer* (IUE—Kondo 1987), the Hopkins Ultraviolet Telescope (Blair et al. 1996), ORFEUS (Barnstedt et al. 2000), and the *Far Ultraviolet Spectroscopic Explorer* (FUSE—Moos et al. 2000) . In addition to these satellites, we can add the Cosmic Origins Spectrograph (COS) on the *Hubble Space Telescope* (HST) since it allows spectroscopy of astronomical objects below *Lyα*.

5.5.1 IUE and HST

For longevity and productivity, the *International Ultraviolet Explorer* and the *Hubble Space Telescope* rank as the most successful missions to date. The IUE satellite, launched in Nov. 1977 (operational from January 1978, through September 1996) was, like *Copernicus*, an exclusively ultraviolet spectroscopic satellite. It consisted of a 45 cm telescope with two absolutely calibrated solar blind spectrographs (1150–2000 Å, 1900–3200 Å) that used two apertures, 10×20 arcsec^2 and 10×10 arcsec^2, and two resolutions (about 300 and 10000). Launched in Nov. 1977 into a geosynchronous orbit, it produced over 10^5 spectra in its lifetime covering sources (Galactic and extragalactic) distributed over most of the sky (see Fig. 5.10). For diffuse ISM studies, it was singularly important for the enormous number of sight lines it probed, in many cases as a collateral product of the primary project. The only limitation was its SIT vidicons detectors (these, unlike CCDs, could physically saturate and were nonlinear at their upper operational range). The archive of all spectra is available through the MAST facility at Space Telescope Science Institute.[5]

HST was launched in Apr. 1990, the first of the NASA Great Observatories program, and is still operating. Placed in a low Earth orbit by the Space Shuttle, it was designed to be serviced by periodic astronaut visits with reboots for its orbit and change-outs for instrument updates. The low orbit, however, reduces its efficiency because of Earth occultations. But that notwithstanding, the complement of high resolution spectrographs carried in the last two decades makes the satellite archive a major resource for interstellar medium studies. The Goddard High Resolution Spectrograph (GHRS) was the first generation high resolution (up to 100,000) single order spectrograph. Its limitation was its detector, an image intensifier coupled to a linear silicon diode array, so only a limited part of the spectrum could be observed at any time. The Space Telescope Imaging Spectrograph (STIS), a second generation instrument on HST, vastly extended capabilities for ultraviolet spectroscopy by using two dimensional detectors (CCDs and Multianode Microchannel Arrays, MAMA) along with echelle gratings extending to resolutions of 100,000 from 1150–3200 Å and medium resolution gratings, R≈30,000.[6]

[5] http://archive.stsci.edu.

[6] The UV spectra shown in Chap. 3 for the nova T Pyx were obtained with STIS.

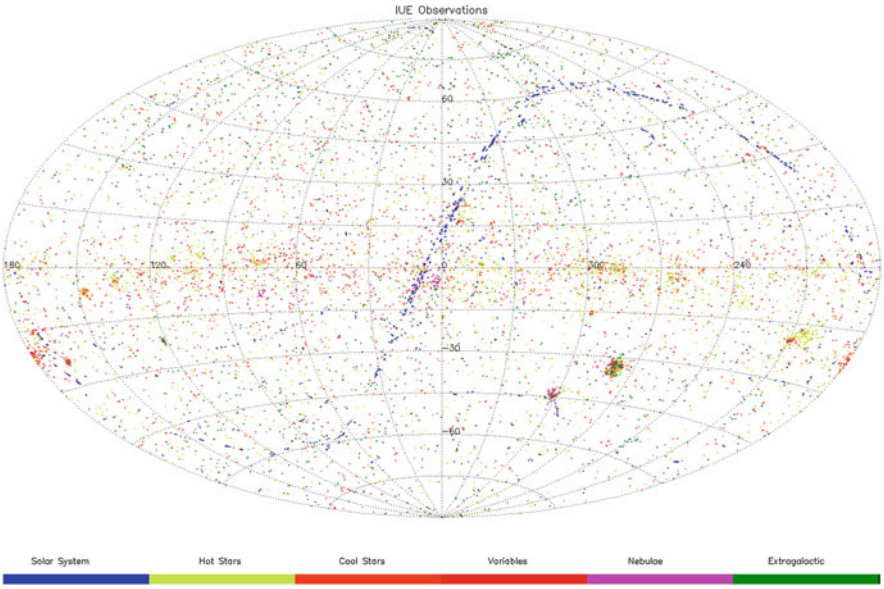

Fig. 5.10 Distribution of lines of sight observed by IUE over its lifetime. The spectrophotometry ranged from high (0.1–0.3 Å) to low (6–7 Å) resolution between 1150 Å and 3200 Å . More than 100,000 UV spectra were obtained with the IUE satellite from January 26, 1978 to September 30, 1996. Image from MAST

5.5.2 FUSE

The FUSE satellite was designed to extend the range of ultraviolet spectroscopy to wavelengths shorter than those detectable by the Hubble Space Telescope (Moos et al. 2000; Sahnow et al. 2000). The satellite was launched in 1999 and remained in operation until 2008. The FUSE instrument channeled the light into 4 channels each of which was comprised of a grating, spectrograph and FUV detector. The four channels overlapped but covered the range from 917–1188 *Å*. This allowed for high-resolution (R $\sim$ 20,000) FUV spectra of hot point sources. A graphical display of the observed lines of sight is shown in figure 5.11. Of particular interest to the diffuse ISM was the presence of several bands of H_2 and CO within FUSE's observable channels. Observations of these lines along the line of sight to various QSOs, Seyferts, BL Lacs, and Galactic Halo stars provided direct, key, information about these molecules in the diffuse ISM.

In particular as far as diffuse molecular gas is concerned, Snow et al. (2000) detected H_2 in the translucent cloud along the line of sight to HD 73882. This initial work was followed up by a more extensive survey towards translucent clouds by Rachford et al. (2002) which primarily studied the correlations between N(H_2) and N(CH), N(CH^+), N(CN), and N(CO). They also noted that many "translucent" lines of sight were really a superposition of several diffuse clouds which combined to produce A_V values greater than 1 magnitude. These lines of

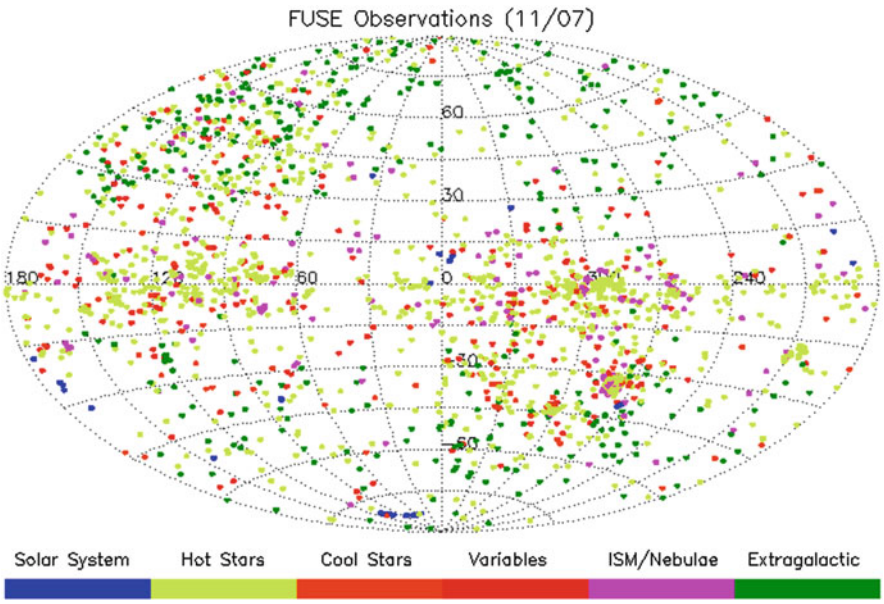

Fig. 5.11 Distribution of lines of sight observed by FUSE over its lifetime (June 24, 1999–October 18, 2007). The Aitoff projection in Galactic coordinates shows nearly 3000 separate astronomical targets that resulted in over 6000 observations. See text for more details. Image from MAST

sight, though "translucent" in the sense that they had substantial extinction, did not represent translucent *clouds*. In this respect, maps of the CO(1-0) line are the best method for identifying these versus a superposition of diffuse clouds along a line of sight (though see discussion in Chap. 7). Richter et al. (2003) surveyed interstellar absorption lines of H_2 in the Lyman and Werner bands toward 56 mostly extragalactic sources. They found N(H_2) values of 10^{14}–10^{17} cm^{-2} in 14 intermediate-velocity clouds (IVCs) in the lower Galactic halo implying that CNM in these clouds is widespread. This result reinforces the idea that virtually any line of sight in the Galaxy has molecules along it, but usually not in sufficient quantities to be deemed a "molecular cloud".

5.6 Probing the X-Ray Sky

X-ray emission is generally associated with compact objects. However, at low X-ray energies (about 1/4 keV) a diffuse background from the HIM is present over most of the sky. As discussed in Chap. 1, the heating for this gas is from supernovae and stellar wind bubbles. At higher energies (above 1/2 keV), this soft background is still visible but it is not as prominent. The isotropy of the radiation at this energy implies an extragalactic origin. Finally, above 1 keV, the diffuse background is likely a superposition of emission from distant extragalactic objects (typically quasars and

AGNs). At the lower energies, nearby dense objects such as molecular clouds can absorb the X-ray emission and produce "shadows" which can be used to study both the absorbing objects and the nature of the more distant emission (e.g., Burrows and Mendenhall 1991).

Like IRAS, ROSAT (operating between 1990 and 1999) was designed to produce an imaging all-sky survey in the soft X-ray range (0.1–2.4 keV) and EUV (0.006–0.2 keV). The PSPC provided a resolution of 20″, and the High Resolution Imager (HRI) achieved 5″. Point source catalogs and diffuse multi-band imaging were not, unlike IRAS, accompanied by spectra. The all-sky maps have an angular resolution of 12′ to highlight the diffuse gas. XMM-*Newton* (launched 1999 and still operating at the time of this book) provides imaging and spectroscopic capabilities. For interstellar studies, the Reflection Grating Spectrometer (RGS) (0.35–2.5 keV) achieves resolutions greater than 100, sufficient to measure ionization edges of abundant species in the diffuse medium when viewed toward bright X-ray sources, providing limits on high ionization state abundances (the presence of very hot diffuse gas). *Suzaku* (2005–2015, see Mitsuda et al. 2007) provided spectrophotometric imaging capabilities with the XIS (Koyama et al. 2007), extending the ROSAT capability in sensitivity and angular resolution while covering a similar energy range. The Swift satellite launched in 2004, and still operating, provides spectrophotometry with the X-ray telescope (XRT) spanning the energy range 0.2–10 keV with a resolution is $\approx$ 40 at 6 keV. This resolution is sufficient to distinguish strong emission lines from point sources and continuum edges, as with XMM-*Newton*. The lower energy range is also especially useful as a probe of the line of sight neutral hydrogen seen against bright sources. Comparing the derived absorption optical depths with 21 cm measurements is especially useful since the continuum absorption is independent of excitation conditions. The *Chandra* x-ray observatory (Tananbaum et al. 2014), launched in 1999 and still operating (2017), is the third of the Great Observatories series. It operates in the 0.09-10 keV range with an effective area of 400 cm^2 with imaging (with better than 1″ resolution) and grating spectroscopy. Because the field of view is small, 31 by 31 $arcmin^2$, ISM studies are best performed on *extragalactic* sources (e.g., imaging of spiral and elliptical galaxies) or targeted study of individual lines of sight (absorption spectroscopy) or broadband imaging of supernova remnants within the Galaxy.

5.7 Probing the Gamma-Ray Sky

Although important milestones in detecting gamma rays from space were achieved with the detectors flown on the NASA SAS-2 and the European COS-B satellites launched in 1972 and 1975, respectively,[7] gamma-ray astronomy really took off with the advent of NASA's *Compton* Gamma-Ray Observatory (CGRO) launched

[7]The first firm detection of Galactic gamma rays was with the experiment flown on the OSO-3 satellite in 1967.

in 1991, the second of the NASA Great Observatories. The failure of a gyroscope on the spacecraft in 2000 caused NASA to deliberately de-orbit the telescope which then crashed into the Pacific Ocean. A review of the discoveries and accomplishments of the mission was given by Gehrels and Shrader (2001). The four instruments on board (BATSE, OSSE, COMPTEL, and EGRET) covered the energy range from 20 keV to 30 GeV with unprecedened resolution and sensitivity. An earlier Franco-Soviet mission, *Granat*, had covered the energy range from 3 keV to 1.3 MeV. Gamma-ray emission from the ISM is produced by cosmic rays interacting with the gas component of the Galaxy (see below); the principal physical processes involved are neutral-pion decay, bremsstrahlung, and inverse Compton scattering. The key instrument on the Compton for wide-field imaging was EGRET; and a whole sky map made with EGRET at > 100 MeV is shown in Fig. 1.3.

In 2008, the *Fermi* Gamma-Ray Space Telescope was launched with new generation instruments: The Gamma-Ray Burst Monitor (GBM) is sensitive to X-rays and gamma-rays in the 8 keV to 40 MeV range and is designed to identify gamma-ray point sources. Although smaller than BATSE, it has the same sensitivity. The imaging instrument is the Large Area Telescope (LAT) which measures the arrival direction, energy, and time of individual gamma rays with energy in the range of 20 Mev to 300 GeV. The LAT's field of view surveys about 20% of the sky at any given time, and scans continuously, covering the whole sky every three hours (two orbits around the Earth). As the images are stacked, ever more sensitive gamma-ray maps of the sky are made. Most gamma-ray sources can be located to within $10'$ and the sensitivity is an order of magnitude better than EGRET. Whole-sky maps of the gamma-ray sky above 1 GeV and 10 GeV can be found at the website of the Fermi LAT collaboration (https://www-glast.stanford.edu/). The Milky Way is prominent in the whole sky maps, a result of the interaction of hydrogen nucleons with cosmic rays. In addition to point sources, the diffuse gamma-ray background comes from the Galaxy and, extragalactically, from unresolved quasars. We describe below how the diffuse galactic gamma-ray background can be used to trace the distribution of H_2.

5.7.1 How Gamma Rays Trace Molecular Gas

G.G. Fazio reviewed in 1967 the principal ways to produce gamma-rays from the Galaxy (Fazio 1967). As far as the diffuse ISM is concerned, cosmic ray nucleons interact with interstellar hydrogen and helium nucleons resulting in gamma-rays with the decay of π^o mesons, cosmic ray electrons interact with the ionized portion of the interstellar gas via bremsstrahlung, and with the interstellar radiation field through the inverse Compton process. In the presence of a magnetic field, cosmic ray electrons can also produce synchrotron radiation. At high energies, the most important emission mechanisms are pion-decay, inverse Compton, and bremsstrahlung. There is a contribution to the diffuse gamma-ray spectrum by an extragalactic component, but it is typically down by a factor of several from the Galactic component in the energy range 20 MeV–20 GeV.

Because most of the high-energy (≥ 50 MeV) interactions occur with interstellar gas, it was quickly realized that studying the diffuse gamma-ray emission at these energies was a way to trace the distribution of Galactic atomic and molecular hydrogen (the helium is assumed to be distributed equally in both phases). The contribution to the diffuse gamma-ray emission from the inverse Compton effect has to be modeled and removed correctly for this technique to work out, but Bloemen (1985) showed how this could be done and concluded that the contribution of inverse Compton gamma rays to the observed gamma-ray diffuse emission was negligible down to 10 MeV. The spectral distributions for pion-decay and electron-bremsstrahlung peak at different energies and so in the 300 MeV–5 GeV range pion-decays dominate.

Given the above considerations, the Galactic diffuse gamma-ray emission can be used to trace directly the column density of molecular hydrogen along a given line of sight. The basic idea is that once the contributions from inverse Compton emission and instrumental effects are removed, the diffuse gamma-ray emission map traces the column density of hydrogen nucleons along a given directions. If the contribution from atomic nucleons is removed (by determining N(HI) from 21 cm data, for example), the remaining gamma ray emission must be from hydrogen in molecular form. The LAT instrument on Fermi should be able to image at least the larger high-latitude molecular clouds and, since they are local objects, would provide information on the local cosmic ray flux. Moreover, observations in varying energy bands can be used with 21 cm data and CO velocity-integrated main-beam antenna temperature data (W_{CO}) to determine the calibration of the CO-H_2 conversion factor. This is discussed further in Sect. 8.2.4.

The high latitude molecular clouds seem like ideal candidates for studies using the technique described above. They are localized and their lines of sight are not confused by foreground and background objects. However, Torres et al. (2005) argued that this population did not have sufficient γ-ray emission to be detected by the EGRET instrument on the CGRO. However, the LAT instrument on the *Fermi* should be able to detect the larger clouds, providing a new way to characterize their H_2 content (see, e.g., Abrahams and Paglione 2015).

References

Abrahams, R.D. and Paglione, T.A.D. 2015, ApJ, 805, 50
Barnstedt, J., Gringel, W., Kappelmann, N., and Grewing, M. 2000, A&AS, 143, 193
Bennett, C.L., et al. 1994, ApJ, 434, 587
Bloemen, J.B.G.M. 1985, A&A, 145, 391
Bohlin, R.C., Savage, B.D., and Drake, J.F. 1978, ApJ, 224, 132
Blair, W.P, Long, K.S., and Raymond, J.C. 1996, ApJ, 468, 871
Boissé, P. et al. 2005, A&A, 429, 509
Boulanger, F., Baud, B., and van Albada, G.D. 1985, A&A, 144, 9
Burrows, D.N. and Mendenhall, J.A. 1991, *Nature*, 351, 629
Carruthers, G. 1970, ApJ, 161, L81
Chaffee, F.H. and Lutz, B.L. 1977, ApJ 213, 349

Chastain, R.J. 2005, PhD Thesis, University of Georgia
Churchwell, E. et al. 2004, PASP, 121, 213
Cotten, D.L. and Magnani, L. 2013, MNRAS, 436, 1152
Crutcher, R.M. and Watson, W.D. 1976, ApJ, 203, L123
Desért, F.X., Boulanger, F., and Shore, S.N. 1986, A&A, 160, 295
Draine, B.T. and Anderson, N. 1985, ApJ, 292, 494
Fazio, G.G. 1967. ARAA, 5, 481
Felenbok, P. and Roueff, E. 1996, ApJ, 465, 57
Fixsen, D.J. et al. 1994, ApJ, 420, 445
Gehrels, N. and Shrader, C.R. 2001, AIPC, 587, 3
IRAS Catalogs and Atlases: Explanatory Supplement 1988, ed. C.A. Beichman, G. Neugebauer, H.J. Habing, P.E. Clegg, and T.J. Chester, Washington, D.C.:GPO
Ingalls, J.G., Bania, T.M., and Jackson, J.M. 1994, ApJ, 431, L139
Ingalls, J.G. 1999, Ph.D. Thesis, Boston University
Ingalls, J.G., Reach, W.T., and Bania, T.M. 2002, 579, 289
Kessler, M.F. et al. 1996, A&A, 315, 27
Kogut, A. et al. 1996, ApJ, 464, L5
Kondo, Y. 1987, *Exploring the Universe with the IUE Satellite*, Astrophysics and Space Science Library, Springer
Koyama, K. et al. 2007, PASJ, 59, 23
Leitch, E.M., Readhead, A.C.S., Pearson, T.J., and Myers, S.T. 1997, ApJ, 486, L23
Low, F.J. et al. 1984, ApJ, 278, L19
Magnani, L. et al. 2003, ApJ, 586, 1111
Mitsuda, K. et al. 2007, PASJ, 59, S1
Miville-Deschênes, M.-A. and Lagache, G. 2005, ApJS, 157, 302
Moos, H.W. et al. 2000, ApJ, 538, L1
Neugebauer, G. et al. 1984, ApJ, 278, L1
Omont, A. 1986, A&A, 164, 159
Planck Collaboration, Planck Early Results XIX, 2011, A&A, 536, A19
Planck Collaboration, Planck Early Results XXI, 2011, A&A, 536, A21
Planck Collaboration, Planck Early Results XXII, 2011, A&A, 536, A22
Planck Collaboration, Planck Early Results XXIII, 2011, A&A, 536, A23
Planck Collaboration, Planck Early Results XXIV, 2011, A&A, 536, A24
Planck Collaboration, Planck Early Results XXV, 2011, A&A, 536, A25
Planck Collaboration, Planck 2013 Results XIII, 2014, A&A, 571, A13
Planck Collaboration, Planck 2015 Results XXVIII, 2014, arXiv:1502.01599
Puget, J.L., Leger, A., and Boulanger, F. 1985, A&A, 142, 19
Rachford, B.L. et al. 2002, ApJ, 577, 221
Richter, P., Wakker, B.P., Savage, B.D., and Semabach, K.R. 2003, ApJ, 586, 230
Sahnow, D.J. et al. 2000, ApJ, 538, L7
Savage, B.D., Bohlin, R.C., Drake, J.F., and Budich, W. 1977, ApJ, 216, 291
Schlegel, D.J., Finkbeiner, D.P., and Davis, M. 1998, ApJ, 500, 525
Sellgren, K. 1984, ApJ, 277, 623
Silverberg, R.F et al. 1993, SPIE, 2019, 180
Smith, A.M. and Stecher, T.P. 1971, ApJ, 164, L43
Snow, T.P., et al. 2000, ApJ, 538, L65
Spitzer, L, Drake, J.F., Jenkins, E.B., Morton, D.C., Rogerson, J.B., and York, D.C. 1973, ApJ, L116
Spitzer, L. 1978, *Physical Processes in the Interstellar Medium*, New York: Wiley-Interscience
Tananbaum, H., Weisskopf, M., Tucker, W., Wilkes, B., and Edmond, P. 2014, RPPhy, 77, 6902
Torres, D.F., Dame, T.M., and Digel, S.W. 2005, ApJ, 621, L29
Weiland, J.P. et al. 1986, ApJ, 306, 101
Werner, M.W. et al. 2004, ApJS, 154, 1
Weselak, T., Galazutdinov, G., Beletsky, Y., and Krelowski, J. 2009, A&A, 499, 783